Journal of Materials, Processing and Design (2025)
Clausius Scientific Press, Canada

DOI: 10.23977/jmpd.2025.090106
ISSN 2516-0923 Vol. 9 Num. 1

The material and structural design of road markings based on radar reflection characteristics

Yu Quan[1,a], Lv Jingjing[1,b,*], Guo Huihui[1,c]

[1]School of Electrical and Control Engineering, North China University of Technology, Beijing, China
[a]194075300@qq.com, [b]TYBJJ2020@hotmail.com, [c]hui6083@qq.com
**Corresponding author*

Keywords: Autonomous driving, Millimeter-wave radar, Lane marking, RCS

Abstract: In response to the critical requirements for lane-keeping in autonomous driving and Advanced Driver Assistance Systems (ADAS), this study focuses on the radar reflection characteristics of road markings, conducting material selection and structural optimization. By establishing a comparative experimental framework for multiple materials, the reflection performance differences of aluminum foil, iron sheets, aluminum particles, and iron powder at the 77 GHz frequency band were evaluated. The optimal material was then selected for structural size optimization, and quantitative evaluation results for various geometric parameters of the samples were obtained. Experimental data show that aluminum foil exhibits significantly better radar cross-section (RCS) characteristics at 77 GHz compared to the other three materials. Furthermore, a reflective structure made of aluminum foil achieved the best reflection effect, with the height (H) having a greater impact on RCS than the length (L). However, as H increases, the effect on RCS gradually diminishes. Changing the incidence angle (β) of all samples results in a decrease in reflection amplitude, but the attenuation is not particularly significant. This confirms the advantage of embedding such structural additive materials into existing road markings for lane detection. Optimal dimensions were H = 8mm, L = 60mm and W=40mm. This study provides a new approach for the identification of road markings by autonomous driving millimeter-wave radar.

1. Introduction

The development of autonomous driving technology began in the 1990s, and after more than two decades of progress, it has evolved from early driver assistance systems to fully automated Level 5 autonomy. Throughout this process, autonomous driving technology has transitioned from single-function capabilities to comprehensive intelligence, continuously improving the vehicle's perception, decision-making, and control abilities. Lane marking detection, as a core task of environmental perception, has become a critical bottleneck affecting system safety due to challenges in reliability and robustness. Traditional vision-based detection methods, such as cameras, perform well under ideal lighting conditions but suffer significant performance degradation in adverse weather conditions such as rain, snow, fog, and haze. Although LiDAR provides high-precision 3D

reconstruction capabilities, its high cost and susceptibility to scattering effects in extreme weather limit its potential for large-scale commercial deployment. Against this backdrop, millimeter-wave radar (mmWave radar) has become a crucial sensing component in most advanced driver assistance systems due to its all-weather operational capability, strong resistance to interference, and cost-effectiveness[1].However, existing road infrastructure, particularly conventional lane markings, has long been designed primarily for human visual recognition. The optical reflection characteristics of traditional marking materials, such as retroreflective glass beads, fail to meet the requirements of radar frequency bands. Their material properties and geometric structures are not optimized for the physical propagation characteristics of radar signals, leaving the potential of radar-based lane detection underutilized. Therefore, optimizing lane marking materials and structural designs to enable lane detection using automotive radar has become a pressing issue in the field of intelligent transportation systems.

Patents[2]and[3]incorporate RFID chips into roads to convey road information. References [4]and[5]integrate magnetic markers into roads, analyzing magnetic field strength for vehicle positioning. However, compared with radar sensors already widely installed on vehicles for ACC, FCW, pedestrian detection, etc., all these methods require installing additional new sensors in vehicles. Reference [6]employs a raised marker for radar detection. However, due to the limitations of the marking material, the radar detection performance is not significant. Moreover, the raised shape of the marking is designed as a strip, without any optimization of its geometry.

In summary, this paper presents several road marking materials, which should have a high dielectric constant or specific electromagnetic characteristics. For cost - effectiveness, this study selects four metal materials: aluminum foil, aluminum granules, iron powder, and iron sheets. By analyzing their radar reflection characteristics and conducting field tests, it compares their radar scattering properties in the 77GHz millimeter - wave band. This helps select optimal materials with high reflectivity and practical feasibility. Furthermore, the study optimizes the material structure for partial or full embedding in road markings, boosting echo intensity. This improves radar recognition accuracy, enabling vehicle - mounted radar to detect lane markings effectively.

The structure of this paper is as follows: Section 2 introduces the preparation of additive material samples and the experimental procedure, where the radar cross-section (RCS) of four different additive materials is compared through eight independent experiments. In Section 3, the RCS characteristics of three different structures are theoretically analyzed, followed by an introduction to the minimum RCS required for radar detection. Additionally, experimental analysis is conducted on the radar reflection characteristics of the optimal structure with varying dimensions. Finally, the last section presents conclusions and future perspectives.

2. Selection of Additive Materials for Lane Marking

2.1. Analysis of Material Properties

In intelligent transportation and autonomous driving systems, the radar detectability of road markings plays a crucial role in vehicle navigation and path planning. To enhance the efficiency of millimeter-wave radar in recognizing road markings, materials with a high radar cross-section (RCS) [7]should be selected. These materials must generate sufficiently strong reflected signals under electromagnetic wave illumination, ensuring that radar can accurately identify the position and boundaries of road markings in complex environments. RCS represents the scattering capability of a target to radar waves and is mathematically expressed as follows:

$$\sigma = \lim_{R\to\infty} 4\pi R^2 \frac{|E_s|^2}{|E_i|^2} \tag{1}$$

where is the RCS value (unit:m^2), is the distance from the radar to the target, and and represent the scattered and incident electric field intensities, respectively. Based on this equation, the RCS values of different materials are calculated to evaluate their radar reflection capabilities.

Iron exhibits high electrical conductivity (approximately 10^7 S/m) and strong electromagnetic wave reflection properties. A continuous metallic surface such as an iron sheet allows for the estimation of its RCS using the physical optics (PO) approximation method.

$$\sigma = \frac{4\pi a^2 b^2}{\lambda^2} \tag{2}$$

Assuming an iron sheet with dimensions of 0.5 m × 0.2 m, at 77 GHz millimeter-wave radar (wavelength $\lambda \approx 3.9mm$), the calculated RCS value of the iron sheet is 25.9 m^2 .

Aluminum, with a higher electrical conductivity of approximately 3.5*10^7 S/m, demonstrates superior electromagnetic reflection properties compared to iron. A continuous aluminum foil surface has an approximated RCS value of 28.5 m^2 .

Since the particle radii of iron powder and aluminum granules are smaller than the wavelength of millimeter-wave radar, the Rayleigh scattering theory is applicable. This theory is suitable for cases where the particle diameter is significantly smaller than the wavelength $(d \ll \lambda)$.In electromagnetic wave scattering theory, the RCS of small particles can be expressed as:

$$\sigma = \frac{\pi^5 d^6}{3\lambda^4} \left| \frac{\varepsilon_r - 1}{\varepsilon_r + 2} \right|^2 \tag{3}$$

Using the Rayleigh scattering model, the calculated RCS values for iron powder and aluminum granules are 2.7×10^{-6} $m^2$and 3.2×10^{-3} m^2, respectively. Based on comprehensive RCS calculations and material properties, the RCS ranking of the four materials is as follows:

$$\sigma_{AluminumFoil} > \sigma_{IronSheet} > \sigma_{AluminumnGramules} > \sigma_{IronPowder}$$

Aluminum foil not only exhibits the highest RCS but also possesses excellent flexibility and weather resistance. Through coating techniques, aluminum foil can be stably adhered to road markings, ensuring reliable radar recognition of lane markings. In contrast, iron sheets are difficult to integrate, and the RCS values of iron powder and aluminum granules are significantly lower than that of aluminum foil, making them unsuitable for efficient radar recognition.

2.2. Sample Preparation and Experimental Procedure

The experiment involves various lane marking additive materials. To ensure the accuracy of the experimental data and eliminate interference from differences in the shapes of the additive materials, a single-variable approach is adopted by standardizing the shape and size of all samples. The sample preparation follows the design shown in (a) Iron Sheet, (b) Iron Powder, (c) Aluminum Granules, (d) Aluminum Foil

Figure 1. Specifically, A4 paper is cut into squares with a side length of 10 cm, and different materials are affixed to these squares using adhesives of uniform thickness and coverage area. This ensures that the sample surface is evenly covered, resulting in multiple sets of experimental samples with different materials.

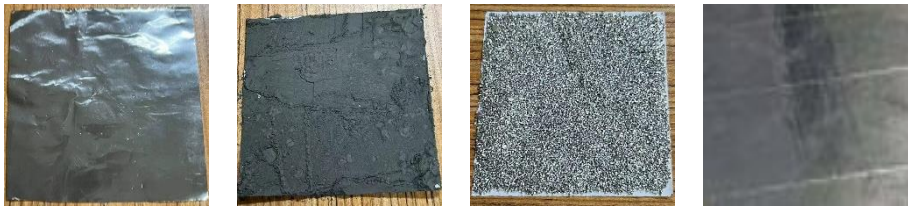

(a) (b) (c) (d)

(a) Iron Sheet, (b) Iron Powder, (c) Aluminum Granules, (d) Aluminum Foil

Figure 1: Test Samples.

During the experiment, to achieve better reflection performance, Figure 2 illustrates the reflection path between the radar and the test samples. The prepared samples are folded 90 ° along one edge. The structural diagram of the test sample is shown in Figure 3.

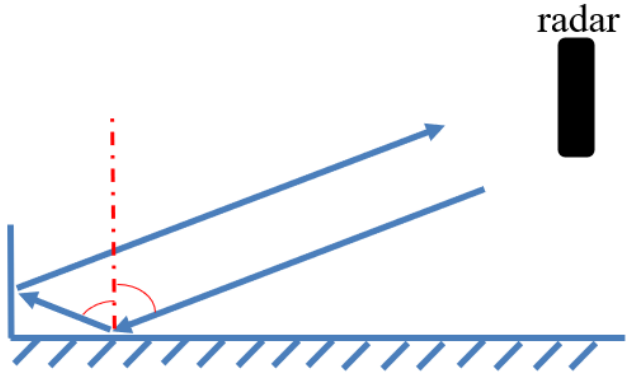

Figure 2: Reflection Path.

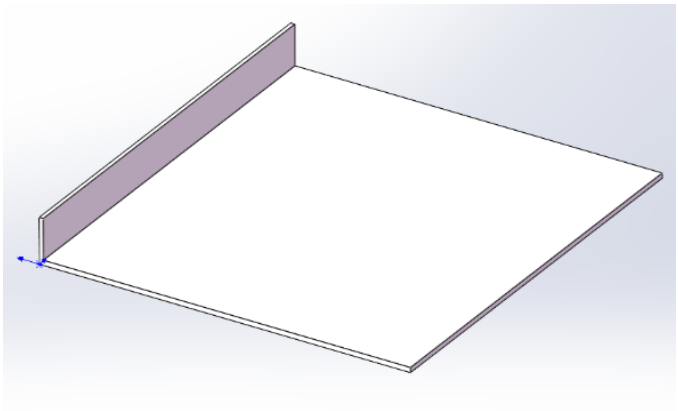

Figure 3: Test Sample Structure.

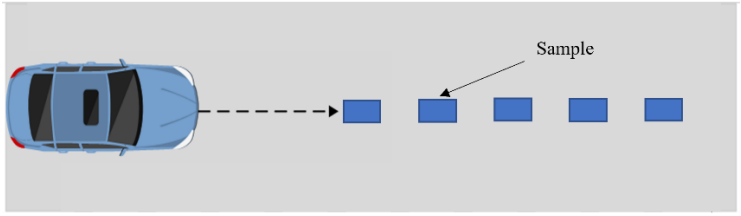

Figure 4: Experimental Scenario Diagram.

The experiment was conducted on an open real-world road using a 77 GHz millimeter-wave radar, minimizing interference from other objects. Taking the iron sheet as an example, the overall

experimental procedure is described as follows. During data collection, both the radar and the test sample remain stationary, maintaining a normal incidence configuration, as shown in Figure 4. First, the test sample is placed at a longitudinal distance of 1 m from the radar. The radar transmits and receives electromagnetic waves, and the received radar data is stored on a computer. The experiment is repeated twice. Next, the test sample is moved to a longitudinal distance of 2 m from the radar, increasing the distance in 1 m increments, and the experiment is repeated at each position until the sample reaches 30 m. After completing the detection of the iron sheet, the same procedure is applied to the other test samples, with experimental data recorded separately for each material.

2.3. Experimental Results

Eight separate experiments compared the Radar Cross Section (RCS) of four added materials, with the same shape and incident angle. Results in Figure 5 show that, at the same shape, size, and incident angle, within 0 - 20 m, aluminum foil had the highest reflectivity, with a maximum RCS of -20 dBsm (about -70 dBsm at 20 m). Iron sheets ranked second, with a small reflectivity gap (around 2 dBsm at 4 m) compared to aluminum foil. Due to their shape, aluminum granules and iron powder caused more radar signal scattering, resulting in much lower reflectivity. The maximum reflectivity of aluminum granules was about 30 dBsm lower than that of aluminum foil, and iron powder was around 40 dBsm lower. Thus, aluminum foil was chosen as the optimal road marking additive. To prevent tire damage, hard aluminum foil was preferred for integration into road markings.

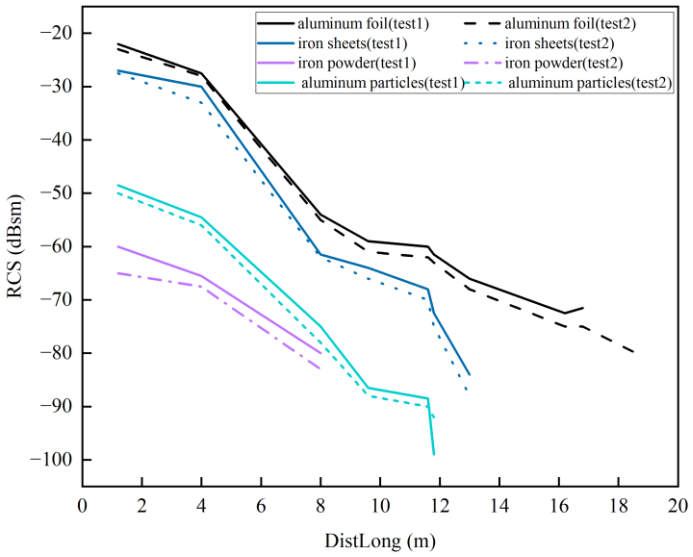

Figure 5: Comparison of Reflection Intensity of Four Metal Materials.

3. Material Structural design

From a structural perspective, specific geometric designs can be implemented to enhance radar wave reflection, similar to the corner reflector structure used in radar reflectors. A corner reflector is a highly efficient passive interference device against radar detection, designed to reflect radio waves directly back to their source. It offers advantages such as a wide operating frequency band, significant interference effects, and high cost-effectiveness, making it widely utilized for the protection of critical military installations and targets[8].A corner reflector typically consists of two or three mutually perpendicular metal panels, which cause incident electromagnetic waves to undergo multiple reflections within the structure. This mechanism ensures that the radar waves are

reflected back in the direction of incidence. Consequently, even small objects with a low inherent RCS can produce sufficiently strong echo signals, resulting in a significantly enhanced radar cross-section[9]. This principle can be leveraged to optimize the radar detectability of road markings in intelligent transportation systems.

3.1. Structural Optimization and Experimental Design

3.1.1. Structural Optimization

As shown in Figure 6, corner reflectors are categorized into three types based on geometry: trihedral (three isosceles right triangles), cubic (three squares), and circular (three circular sectors with a 90 ° central angle). Each surface of these reflectors can be considered an ideal PEC (Perfect Electric Conductor) plate[10].

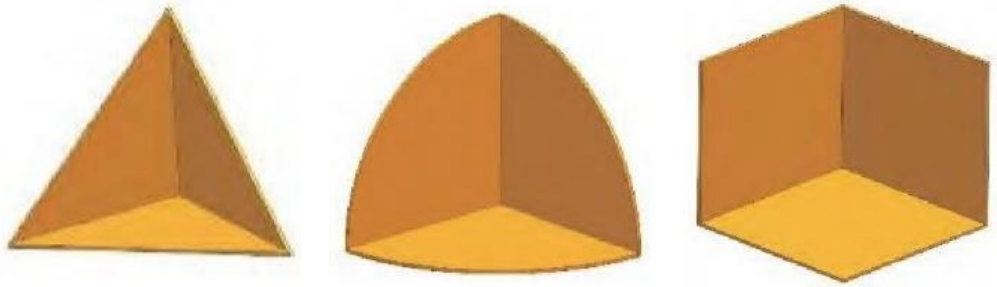

(a)Triangle (b)Circle (c)Square

Figure 6: Three typical corner reflectors.

The maximum RCS of the corner reflector for electromagnetic waves incident along its symmetry axis can reach the theoretical value[11].

$$\sigma_{\max} = \frac{4\pi A_r^2}{\lambda^2} \tag{4}$$

In the formula, A_r is the projection area perpendicular to the electromagnetic wave, as shown in Figure 7. The regions near the three vertices of the triangular corner reflector have little impact on its RCS. Instead, the maximum RCS depends on the hexagonal area inside, with a side length of l/3 that varies with the incident angle. The maximum effective area is:

$$A_r = \frac{a^2}{2\sqrt{3}} \tag{5}$$

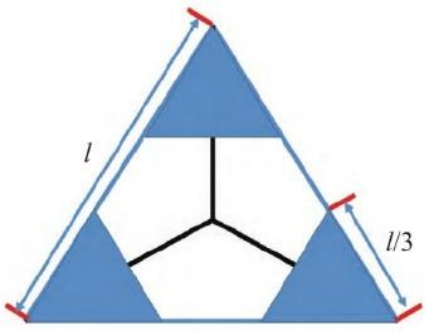

Figure 7: Projection Diagram.

In the formula, a is the edge length of the corner reflector. Thus, the maximum RCS of a triangular corner reflector can be obtained as:

$$\sigma_{\max} = \frac{4\pi a^4}{3\lambda^2} \tag{6}$$

The radar reflection performance varies with the shape of the radar corner reflector. The performance parameters of the above three types of radar reflectors are shown in Table 1:

Table 1: Basic Performance Parameters of Three Types of Radar Corner Reflectors.

Type	Beamwidth	Maximum RCS	Average RCS
Triangle	40	$\frac{4\pi a^4}{3\lambda^2}$	$\frac{0.7a^4}{\lambda^2}$
Square	23	$\frac{12\pi a^4}{\lambda^2}$	$\frac{0.47a^4}{\lambda^2}$
Circle	32	$\frac{15.6a^4}{\lambda^2}$	$\frac{0.17a^4}{\lambda^2}$

After comparing the performance of three common corner reflectors, it is evident that the square corner reflector outperforms the triangular corner reflector in terms of maximum radar cross-section (RCS) and surpasses the circular reflector in terms of average RCS. Although its beamwidth is relatively narrow, this characteristic can be advantageous in specific scenarios where enhanced reflection in a particular direction is desired. For instance, in road marking applications, maximizing the echo signal from vehicle radar is crucial for improving detection performance. To accommodate detection at multiple angles, two parallel corner reflectors can be placed on opposite sides of the marking, ensuring greater echo power over a wider range of incidence angles.

Therefore, in designing a new road marking enhancement structure, this study selects the square corner reflector as the fundamental unit, leveraging its larger RCS to enhance radar signal reflection. Additionally, the geometric configuration of the structure is optimized, as illustrated in the Figure 8.

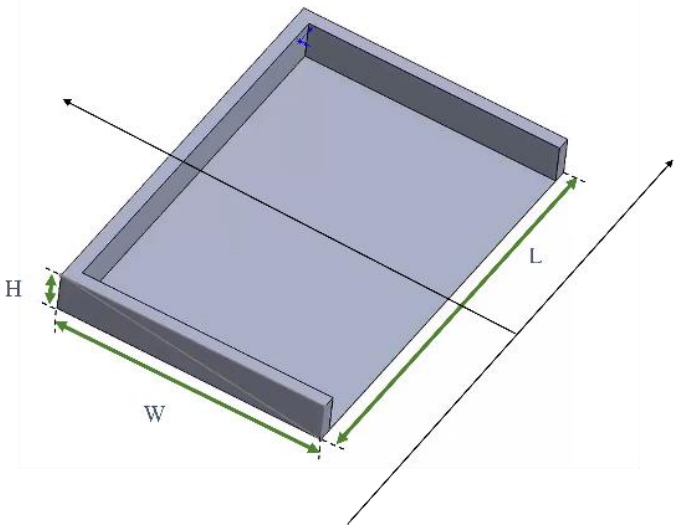

Figure 8: Structural Design.

The added material test sample is simply deployed onto existing road markings, following the standard of raised pavement markings. The width W of the added material is set to 40 mm, allowing for a broader incidence angle range. Furthermore, the base of the reflector is extended to increase the reflective surface area, enabling partial or full embedding within the road marking. This design ensures improved radar detection of road markings without interfering with normal vehicle operation. Based on this initial design, further optimizations of the height and length of the new structure are conducted to enhance the strength of the radar echo signal.

3.1.2. Experimental Design

Select a spacious test site with minimal electromagnetic interference to reduce the impact of unwanted reflections on radar signals during testing. The automotive millimeter-wave radar is securely mounted at the front of the test vehicle, and test samples of varying sizes (length L, height H) are prepared.

(1) Reflection Intensity Testing

To evaluate the impact of different material dimensions on radar signal reflection, multiple test samples are designed and experimentally verified. This study optimizes the length and height of the added material to identify the optimal design that meets the radar's RCS detection requirements, providing a reference for future material enhancements.

In the experimental design, the first step is to fix the sample length at 60 mm while varying the sample height to assess its influence on radar cross-section (RCS). The goal is to determine the optimal height that satisfies the minimum RCS requirement. The height range is set between 3 mm and 10 mm, with specific design details outlined in the table 2 below.

Table 2 Height design

Sample	L(mm)	**H(mm)**
Sample 1	60	3
Sample 2		4
Sample 3		5
Sample 4		6
Sample 5		7
Sample 6		8
Sample 7		9
Sample 8		10

Furthermore, to analyze the effect of length on the reflective performance of the added material, samples with a fixed height of 6 mm are designed for comparative study. The sample length starts at 20 mm and gradually increases to 200 mm. Experimental data are then used to evaluate their reflection characteristics. The specific design details are presented in the table 3 below.

Table 3: Width design

Sample	H(mm)	**L(mm)**
Sample 1	6	20
Sample 2		40
Sample 3		60
Sample 4		80
Sample 5		100
Sample 6		120
Sample 7		140
Sample 8		160
Sample 9		180
Sample 10		200

For each test sample size, the sample is adjusted to face the millimeter-wave radar system directly, corresponding to an incidence angle of 0 °. The radar system is then activated to transmit millimeter-wave radar signals toward the test sample, and the intensity of the reflected signal is recorded. Each reflector size is measured three times, and the average value is taken as the reflection intensity at the direct-facing angle.

This experiment evaluates the impact of different material heights and lengths on RCS, collecting reflection performance data for each sample size. By analyzing variations in height while keeping the length fixed and examining length variations at a fixed height, a foundation is established for further data analysis. The experimental results will be thoroughly compared and discussed in subsequent sections to determine the optimal design and provide insights for further refinement of the added material.

(2) Angle Dependence Testing

Since test samples will encounter different angles as vehicles move, adjusting the test sample's angle is necessary. The samples are initially positioned at the direct-facing angle (0 °) and gradually rotated in increments of 10 °, 20 °, and 30 ° to simulate different incidence angles. The reflection intensity is measured at each incidence angle, and for each angle, three repeated measurements are conducted for all sample sizes to ensure data reliability.

The reflection intensity variation with incidence angle is plotted to analyze the angular dependence of different sample sizes. At each angle, the radar measures the reflection intensity of the test sample, and three repeated experiments are conducted for each sample size to enhance data reliability. After recording the experimental data, the average reflection intensity at each angle is calculated, and a curve showing reflection intensity as a function of incidence angle is plotted for a visual representation of angular effects on reflection performance. Finally, by analyzing the reflection characteristics of different sample sizes across varying angles, the angle dependence is examined, and the optimization effects of different sample sizes are compared.

3.2. Results and Analysis

3.2.1. Reflection Intensity Test Results

To clearly present the relative relationships among different sample sizes and quickly identify the optimal size range, reflection intensity is normalized. All results are normalized relative to the maximum reflection amplitude within their respective groups, with the reflection intensity at the maximum height (H) and length (L) set to 0.

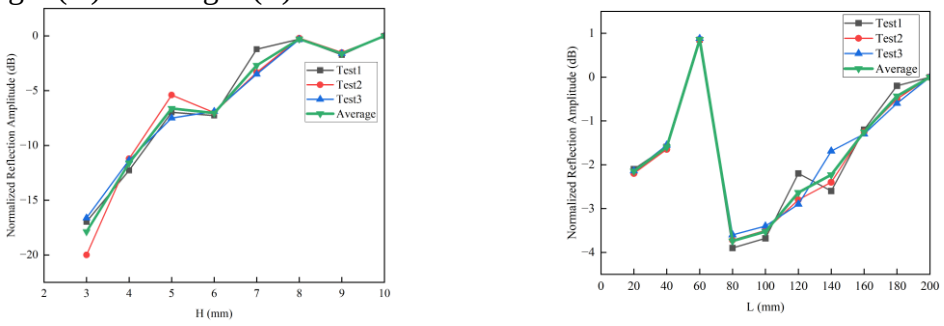

(a) (b)

Figure 9: Reflection Amplitudes and Mean Values at Different Heights (H) and Lengths (L) Across Three Experiments (β = 0°).

Figure 9 shows the effect of height (H) and length (L) on reflection amplitude. As height (H) increases, the reflection amplitude rises by approximately 18 dB within the range of 3 mm to 10

mm. Beyond 8 mm in height, the impact on reflection amplitude diminishes. For example, when H changes from 3 mm to 5 mm, the reflection amplitude increases by about 10 dB, while when H changes from 9 mm to 10 mm, the reflection amplitude only increases by about 2 dB. Thus, it can be concluded that further increasing height (H) does not significantly improve reflection performance.

In contrast to the effect of height (H) on reflection amplitude shown in Figure (a), Figure (b) illustrates the impact of length (L) on reflection amplitude. The amplitude difference for different lengths (L) is relatively small. When L changes from 20 mm to 200 mm, the reflection amplitude difference is about 2 dB. In summary, height (H) has a greater influence on reflection amplitude compared to length (L). As the sample height (H) increases, the effect on reflection amplitude becomes progressively smaller.

3.2.2. Angle Dependence Test Results

For the angle dependency test of the added material, experiments were conducted according to the experimental design. The reflected signal strength was measured at different incidence angles. For each incidence angle, experiments were repeated three times for samples with varying heights (H) and lengths (L), and the data were recorded accordingly. The reflection amplitudes and their averages under $\beta = 10°$ for different H and L values are shown in Figure 10. Similarly, the results for $\beta = 20°$ and $\beta = 30°$ are presented in Figures 11 and 12, respectively. A curve illustrating the variation of reflection intensity with incidence angle was plotted to analyze the angle dependency of the test samples with different dimensions. The reflection intensities were normalized, as shown in Figure 13, where all results were normalized with respect to the maximum reflection amplitude within each group. The reference point was set at $\beta = 0°$, and its value was defined as zero.

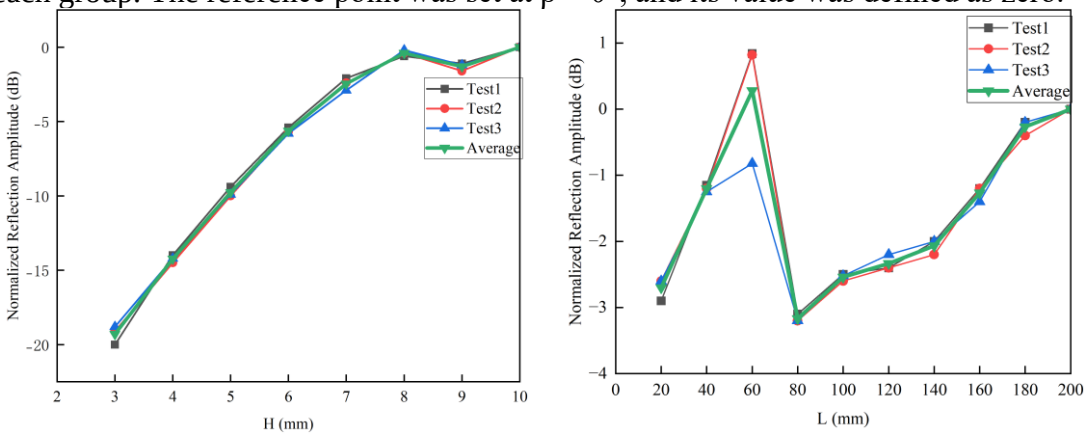

Figure 10: Reflection Amplitudes and Mean Values at Different Heights (H) and Lengths (L) Across Three Experiments ($\beta = 10$ °).

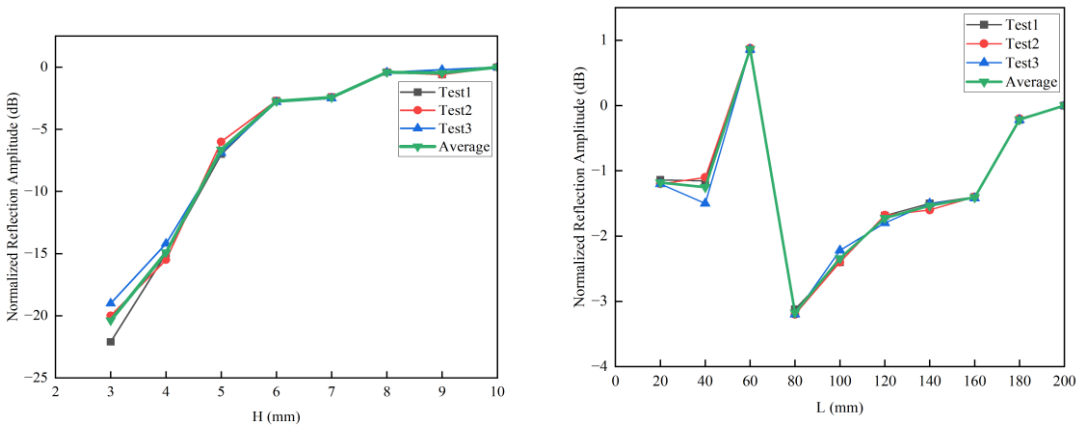

(a) (b)

Figure 11: Reflection Amplitudes and Mean Values at Different Heights (H) and Lengths (L) Across Three Experiments (β = 20°).

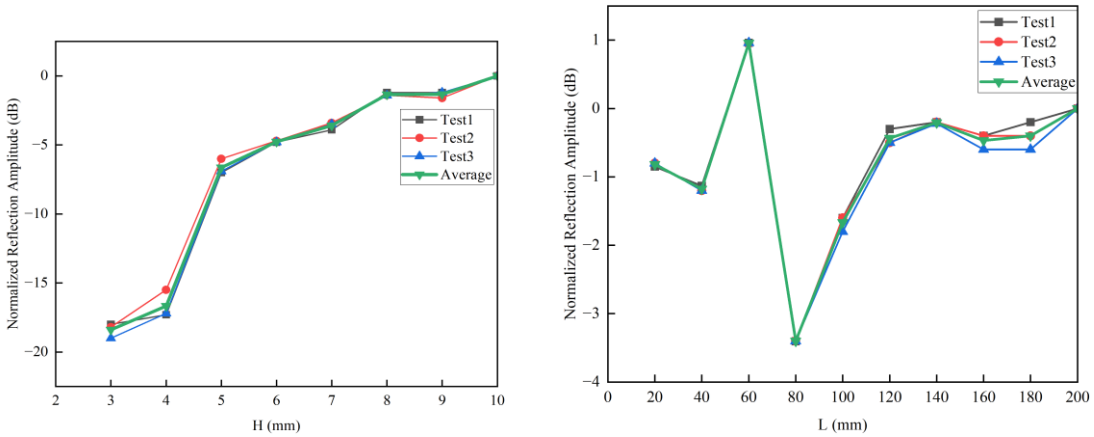

(a) (b)

Figure 12: Reflection Amplitudes and Mean Values at Different Heights (H) and Lengths (L) Across Three Experiments (β = 30°).

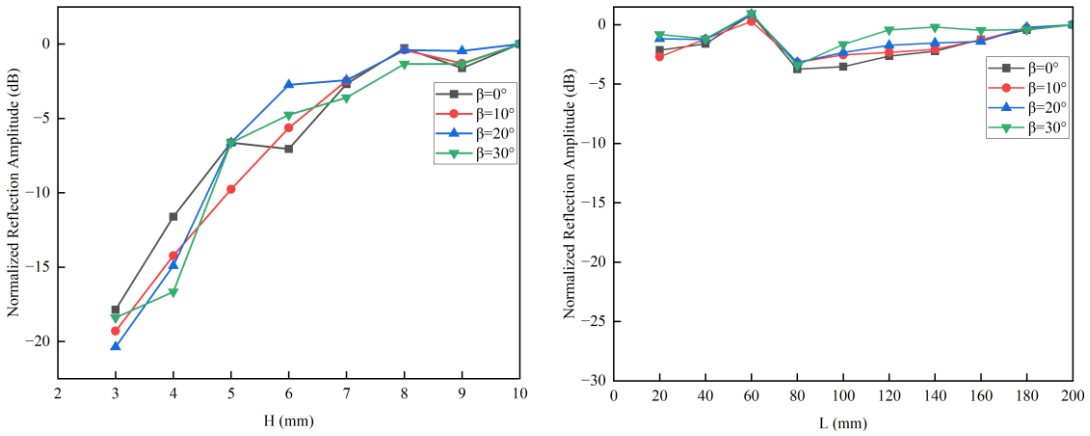

(a) (b)

Figure 13: The Effect of Different Incidence Angles and Different Sizes on Reflection Amplitude.

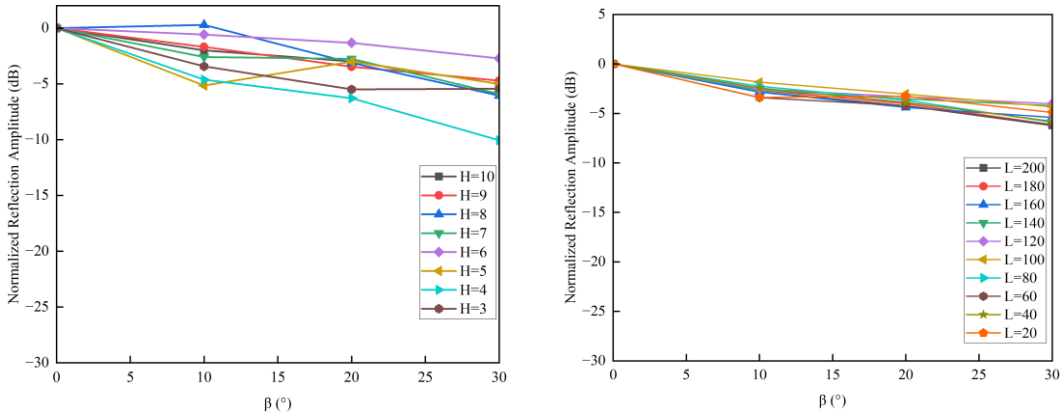

(a) (b)

Figure 14: The Relationship Between Reflection Amplitude and Azimuth Angle for Different Sizes.

The reflection dependence on β for samples of different sizes in Figure 14 indicates that as β increases from 0 ° to 20 °, the reflected signal strength decreases by approximately 1–6 dB for samples with different heights (H). When β increases from 0° to 30°, the signal strength decreases by approximately 3–10 dB. For samples with different lengths (L) in Figure 14(b), the reflected signal strength decreases by about 3 dB as β increases from 0° to 20°, and by approximately 3–6 dB when β increases from 0° to 30 °.

In summary, changing the incidence angle β for all samples results in a decrease in reflection amplitude, but the effect is not particularly significant. This also demonstrates the advantage of embedding such structural added materials in existing road markings for lane detection. Based on practical application scenarios and cost considerations, a four-sided structure with a height (H) of 8 mm, length (L) of 60 mm, and width (W) of 40 mm can be selected to form an innovative road marking suitable for millimeter-wave radar recognition.

4. Conclusions

This study proposes an innovative road marking enhanced by millimeter - wave radar for detection. The selection of materials, structural design, and size optimization ensure maximum radar reflectivity when embedded in traditional markings. If the height (H) of the optimal reflective material, aluminum foil, is much smaller than its length (L), H significantly impacts the Radar Cross Section (RCS), with this impact diminishing as H increases. Changing the incidence angle (β) of all samples results in a decrease in reflection amplitude, but the attenuation is not particularly significant. This confirms the advantage of embedding such structural additive materials into existing road markings for lane detection. This research offers insights into creating road markings with enhanced millimeter - wave radar recognition.

References

[1] Thakur R . Scanning LIDAR in Advanced Driver Assistance Systems and Beyond: Building a road map for next generation LIDAR technology[J]. IEEE Consumer Electronics Magazine, 2016, 5(3).

[2] O. Bogatine, "Tracking lane marker position through use of information-transmiting device," U.S. Patent 20120098657 A1, Apr. 26, 2012.

[3] W. McCarthy, K. H. White, and G. Sill, "Pavement marking tape incorporating advanced materials for improved visibility," U.S. Patent 20160209559 A1, Jul. 21, 2016.

[4] C.-Y. Chan and H.-S. Tan, "Evaluation of magnetic markers as a position reference system for ground vehicle guidance and control," California Partners Adv. Transp. Technol., Univ. Berkeley, Berkeley, CA, USA, Tech. Rep. UCB-ITS-PRR-2003-8, 2003.

[5] J. I. Hernandez and C.-Y. Kuo, "Steering control of automated vehicles using absolute positioning GPS and magnetic markers," IEEE Trans. Veh. Technol., vol. 52, no. 1, pp. 150–161, Jan. 2003
[6] Nakamura H, Ushiro K. Development and verification of a lane marker detection system in all-weather conditions[J]. JARI Res. J, 2017: 1-6.
[7] Zhang Zhiyuan, Zhang Jieqiu, Qu Shaobo, et al. Research Progress and Prospects of Radar Corner Reflectors [J]. Cruise Missile, 2014(4): 64-70.
[8] Chen Yan, Wang Zhanling, Xiao Ke, et al. Design and Scattering Characteristic Analysis of a Novel Variable-Polarization Corner Reflector [J]. Journal of Electromagnetic Waves, 2023, 38(6): 913-920.
[9] Chen Jing. Principles of Radar Passive Interference [M]. Beijing: National Defense Industry Press, 2009: 84-87.
[10] Zhao Feiyu, Yu Qun, Niu Shuai, et al. Electromagnetic Scattering Characteristic Analysis and Application of Atypical Polyhedral Corner Reflectors [J]. Journal of Electromagnetic Waves, 2023, 38(6): 982-988.
[11] Sukharevsky O I, Vasliets V A, Nechitaylo Sv. Scattering characteristics computation method for corner reflectors in arbitrary illimination conditions[C]//International Conference on Antenna Theory and Techniques, Kharkiv, Ukraine, Apr. 21-25, 2015.